# Energetics and diffusion of intrinsic surface and subsurface defects on anatase $TiO_2(101)$

Hongzhi Cheng, and Annabella Selloni

**Articles you may be interested in**

Excess electron states in reduced bulk anatase $TiO_2$: Comparison of standard GGA, $GGA + U$, and hybrid DFT calculations
The Journal of Chemical Physics **129**, 154113 (2008); 10.1063/1.2996362

Influence of external electric fields on oxygen vacancies at the anatase (101) surface
The Journal of Chemical Physics **141**, 084705 (2014); 10.1063/1.4893559

Reaction pathway and free energy barrier for defect-induced water dissociation on the (101) surface of $TiO_2$-anatase
The Journal of Chemical Physics **119**, 7445 (2003); 10.1063/1.1607306

A climbing image nudged elastic band method for finding saddle points and minimum energy paths
The Journal of Chemical Physics **113**, 9901 (2000); 10.1063/1.1329672

Electronic structure of anatase $TiO_2$ oxide
Journal of Applied Physics **75**, 2945 (1994); 10.1063/1.356190

Ab-initio study of hydrogen doping and oxygen vacancy at anatase $TiO_2$ surface
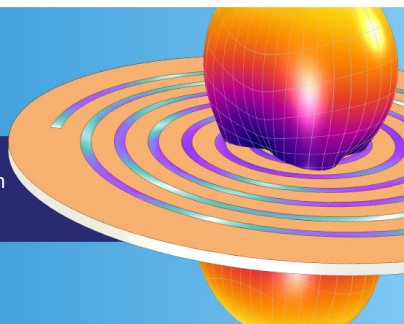AIP Advances **4**, 027129 (2014); 10.1063/1.4866982

# Energetics and diffusion of intrinsic surface and subsurface defects on anatase TiO$_2$(101)

Hongzhi Cheng and Annabella Selloni[a)]
*Department of Chemistry, Princeton University, Princeton, New Jersey 08544, USA*

We report on density functional theory (DFT) calculations of the formation energies and diffusion pathways of oxygen vacancies and Ti interstitials at and near the (101) surface and in the bulk of the anatase polymorph of TiO$_2$. At the generalized gradient approximation level, both defects are found to be energetically more stable by $\sim$0.5 eV or more at bulk and subsurface sites than on the surface. Moreover, the energy barriers to diffuse from the surface to the bulk are rather low, while the opposite is true for the barriers to diffuse from the bulk to the surface. This indicates that similar to Ti interstitials, also oxygen vacancies should preferentially occur at subsurface rather than at surface sites. To substantiate these findings, additional DFT+$U$ calculations have been performed using different values of $U$ in the range $2.5 \le U \le 4.5$ eV. These show small differences in the relative stabilities of surface and subsurface oxygen vacancies with subsurface vacancies being more stable at low $U$ values and a crossover in stability taking place around $U \sim 3$ eV. Analogous calculations for the TiO$_2$(110) surface of rutile show that surface bridging oxygen vacancies are largely favored with respect to subsurface vacancies for all values of $U$. Altogether, our results provide evidence of important differences between reduced anatase and rutile surfaces in agreement with recent experimental observations. © *2009 American Institute of Physics*. [DOI: 10.1063/1.3194301]

## I. INTRODUCTION

Intrinsic point defects strongly affect the physical and chemical properties of metal oxides. In heterogeneous catalysis, the adsorption of molecular species and/or metal particles is usually initiated at surface defect sites. In photocatalysis, a field where oxide semiconductors are widely used, defects can favor the surface reactivity but can also have a detrimental effect by acting as recombination centers or traps for the photoexcited carriers. Excess carriers generated by bulk vacancies and interstitials largely determine the electrical properties and/or the color of semiconducting and insulating oxides. The diffusion of point defects has a key role in the mass transport occurring between the surface and the bulk in various surface preparation processes such as sputtering and annealing.

It is evident from the above examples that the role and properties of defects also depend on their locations, i.e., on whether they are at surface, subsurface, or bulk sites. For this reason, knowing how defects are distributed among these different sites can be very useful. Under equilibrium conditions, the concentration $c$ of an intrinsic point defect, either an interstitial or a vacancy, is related to its formation energy $E_{\text{form}}$ via the simple expression

$$c = N_{\text{sites}} \exp(-E_{\text{form}}/k_B T), \tag{1}$$

where $k_B$ is Boltzmann's constant, $T$ is the temperature (in °K), and $N_{\text{sites}}$ represents the density of lattice sites where the defect can form. While it is generally reasonable to assume that $N_{\text{sites}}$ is the same at the surface and in the subsur-

face region of the material, the formation energies of subsurface and surface defects can be quite different simply because surface and subsurface atoms have a different coordination or, more generally, a different environment. In particular, the formation energies of vacancies are usually expected to be lower at the surface, where a smaller number of bonds need to be broken, whereas interstitials generally prefer a highly coordinated environment and are thus more stable in the subsurface and bulk regions than at the surface. The difference in surface versus subsurface formation energies can then lead to different defect concentrations at and away from the surface of the material.

In this work, we theoretically investigate the energetics and diffusion of intrinsic point defects at various surface and subsurface sites of anatase-TiO$_2$ (A-TiO$_2$), a technologically important metal oxide semiconductor that is widely applied in photocatalysis[1–3] and solar energy conversion.[4,5] In particular, we consider oxygen vacancies ($V_O$s) and Ti interstitials (Ti$_i$s) at and near the A-TiO$_2$(101) surface, which is the lowest energy and most frequently exposed surface of A-TiO$_2$.[6,7] On this surface, atomically resolved scanning tunneling microscopy (STM) measurements show the presence of a low density of O vacancies compared to the typical number density of 5%–10% that is observed on the much studied rutile R-TiO$_2$(110) surface under similar preparation conditions.[8,9] Consistent with these observations, water temperature programmed desorption (TPD) data for the same A-TiO$_2$(101) surface do not show the $\sim$500 K feature that characterizes the recombinative desorption of dissociated molecules at defect sites, as observed for R-TiO$_2$(110).[10] Vice versa, ultraviolet photoemission spectroscopy (UPS) measurements[11] indicate that the concentration of O vacan-

a)Electronic mail: aselloni@princeton.edu.

cies is quite large at the A-TiO$_2$(101) surface compared to R-TiO$_2$(110) under the same preparation conditions. It should be noted, however, that the O-vacancy states detected by UPS originate not only by the defects that are exactly at the surface but also by those in a few layers below. Thus, investigation of the energetics of surface and subsurface defects is also important for clarifying the apparent contrast between the STM/TPD and UPS data.

The present study of surface and subsurface defects at A-TiO$_2$(101) employs both density functional theory-generalized gradient approximation (DFT-GGA) and DFT+$U$ calculations. As discussed in several recent studies,[12–15] DFT-GGA shows important limitations in the description of the electronic structure of intrinsic point defects in TiO$_2$. For O vacancies, in particular, this approach predicts that the defect-induced electronic states lie at the bottom of the TiO$_2$ conduction band,[12–14,16] whereas experiments indicate that these states are in the TiO$_2$ band gap at energies of $\sim 0.8-1.0$ eV *below* the bottom of the conduction band.[11,17,18] These difficulties of DFT-GGA are believed to mostly originate from the self-interaction error of the approximate DFT functionals[19] and can be mitigated by the use of hybrid functionals or DFT+$U$ methods.[19,20] The available theoretical investigations of O vacancies in TiO$_2$ based on the latter approaches[12–15,21] show indeed the occurrence of localized states in the band gap; these states are associated with a local distortion of the lattice, i.e., have a polaronlike character. We have thus applied the DFT+$U$ approach (hybrid functional calculations are very cumbersome for the large systems of interest in this work) to investigate how the relative stability of surface and subsurface $V_O$ defects on A-TiO$_2$(101) is affected by the localized versus delocalized character of the defect states. Specifically, we have performed spin-polarized DFT+$U$ calculations using $U$ values ($2.5 \leq U \leq 4.5$ eV) that encompass the range of values typically considered as most realistic for TiO$_2$.[15,21,22] For comparison we carried out similar DFT-GGA and DFT+$U$ calculations of surface and subsurface O vacancies also for the R-TiO$_2$(110) surface.

For A-TiO$_2$(101), our DFT-GGA calculations show that *both* Ti$_i$ and $V_O$ defects are significantly more stable at subsurface than at surface sites. (Some of the results on $V_O$ defects have been already reported in Ref. 23.) By contrast, analogous calculations for O vacancies at R-TiO$_2$(110) show that the formation energy of surface twofold bridging oxygen (O$_{2c}$) vacancies is much smaller than that of subsurface defects.[24–26] For A-TiO$_2$(101), in addition, the energy barriers to diffuse from the surface to the bulk are rather low, while the opposite is true for the barriers to diffuse from the bulk to the surface. Diffusion barriers are particularly low (less than 0.5 eV) for Ti$_i$ defects; thus these species are expected to have an important role during annealing processes, even though the computed formation energies indicate that O vacancies should be much more numerous under equilibrium conditions.

As for DFT+$U$ calculations, we found that for A-TiO$_2$(101) the relative stability of surface and subsurface vacancies depends on the value of $U$ with a crossover in stability occurring at $U \sim 3$ eV. For R-TiO$_2$(101), instead,
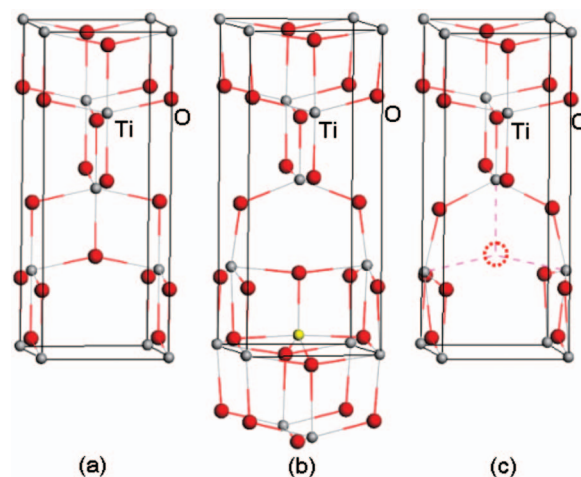


FIG. 1. (a) Unit cell of bulk anatase, (b) DFT-GGA relaxed atomic structures of a Ti interstitial, and (c) an O-vacancy defect in bulk anatase. In (b) the Ti interstitial is yellow; in (c) the dashed red circle indicates the position of the oxygen atom before it was removed to form a vacancy. The O atoms are red and Ti atoms are gray.

bridging oxygen vacancies are always favored for all investigated values of $U$. Despite the differences between the DFT-GGA and GGA+$U$ results, our study clearly indicates that subsurface O vacancies are substantially more important at A-TiO$_2$(101) than at the R-TiO$_2$(110) surface.

This paper is organized as follows. After presenting our computational approach (Sec. II), in Sec. III we report the results of our DFT-GGA calculations. We start with the formation energies and diffusion pathways of Ti$_i$ and $V_O$ defects in bulk A-TiO$_2$ (Sec. III A) and next discuss surface and subsurface binding sites and associated diffusion pathways for Ti interstitials (Sec. III B) and O vacancies (Sec. III C). In Sec. IV, we report on our GGA+$U$ calculations of the relative stability of surface and subsurface vacancies. Results for rutile are presented in Sec. V while our conclusions are given in Sec. VI.

## II. COMPUTATIONAL SETUP

The DFT-GGA calculations have been carried out using the Perdew-Burke-Ernzerhof (PBE) (Ref. 27) exchange-correlation functional within the plane-wave-pseudopotential scheme;[28] the effect of spin polarization has been extensively tested and found to be irrelevant in the case of anatase for which the singlet and triplet solutions are essentially degenerate at the GGA level. The PBE functional was used also for the spin-polarized DFT+$U$ calculations with 2.5 eV$\leq U$ $\leq 4.5$ eV. Ultrasoft pseudopotentials[29] and a kinetic energy cutoff of 25 (200) Ry for the smooth part of the wave functions (augmented density) were used.

The anatase (101) surface was modeled using a repeated slab geometry with a vacuum of $\sim 11.5$ Å width between slabs. The computed bulk lattice parameters $a = 3.77$ Å and $c = 9.54$ Å (experimental values:[30] $a = 3.782$ Å and $c = 9.502$ Å) were obtained by relaxing a tetragonal bulk unit cell containing four TiO$_2$ units and sampling the corresponding Brillouin zone with a $5 \times 5 \times 2$ mesh of $k$-points. We considered slabs of three TiO$_2$ layers with
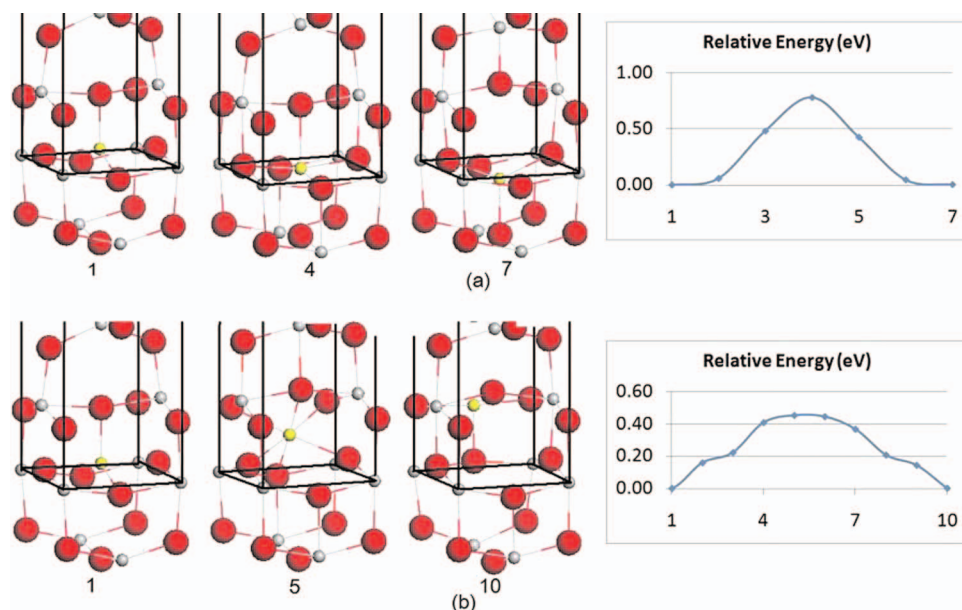
FIG. 2. Diffusion pathways and corresponding potential energy barriers for a Ti interstitial in bulk anatase: (a) along the [001] direction and (b) along the [301] direction. Integers denote the different images in the NEB calculations of the pathways. The O atoms are red, Ti atoms are gray, and Ti interstitial is yellow.

$1 \times 2$ ($10.26 \times 7.54$ Å$^2$) and $1 \times 3$ ($10.26 \times 11.31$ Å$^2$) surface supercells containing 72 and 108 atoms, respectively, as well as a thicker slab of six TiO$_2$ layers, again with $1 \times 3$ surface supercell containing 216 atoms. The GGA+$U$ calculations were performed on A-TiO$_2$(101) slabs of four TiO$_2$ layers with 96 and 144 atoms. Due to the large sizes of these systems, only $\Gamma$ was used to sample $k$-space; test calculations on the 72-atom slab showed negligible ($\sim$0.03 eV) differences between the formation energies of surface and subsurface defects determined with a $2 \times 2 \times 1$ $k$-point mesh and those obtained using only $\Gamma$. In the structural optimizations, all the atoms of the slab, except those in the bottom layer, were allowed to move (force threshold: 0.05 eV/Å).

Diffusion pathways and barriers were calculated only at the DFT-GGA level using the nudged-elastic-band (NEB) method;[31] for each set of initial and final states different pathways were explored in order to determine the most favorable one.

To determine the formation energies ($E_{\text{form}}$) of Ti$_i$ and $V_O$ defects, we assume the system to be in thermodynamic equilibrium with both a reservoir of oxygen (of chemical potential $\mu_O$) and a reservoir of bulk TiO$_2$ (of chemical potential $\mu_{\text{TiO}_2}$); it is also convenient to refer $\mu_O$ to the energy $E_{\text{tot}}$ of an O atom in O$_2$, i.e., $\mu_O \equiv 1/2 E_{\text{tot}}(O_2) + \mu'_O$. This gives

$$E_{\text{form}}(\text{Ti}_i) = G(\text{def}) - G(\text{no-def}) - \mu_{\text{TiO}_2} + E_{\text{tot}}(O_2) + 2\mu'_O, \tag{2}$$

$$E_{\text{form}}(V_O) = G(\text{def}) - G(\text{no-def}) + 1/2 E_{\text{tot}}(O_2) + \mu'_O, \tag{3}$$

where $G$ (def) and $G$ (no-def) are the free energies of the system with and without defects, respectively, and $\mu'_O$ is constrained to $1/2\, H_f \leq \mu'_O \leq 0$, where $H_f$ is the low-temperature heat of formation of A-TiO$_2$.[32] As in most theoretical studies of defect formation energies in TiO$_2$, we restrict to the value
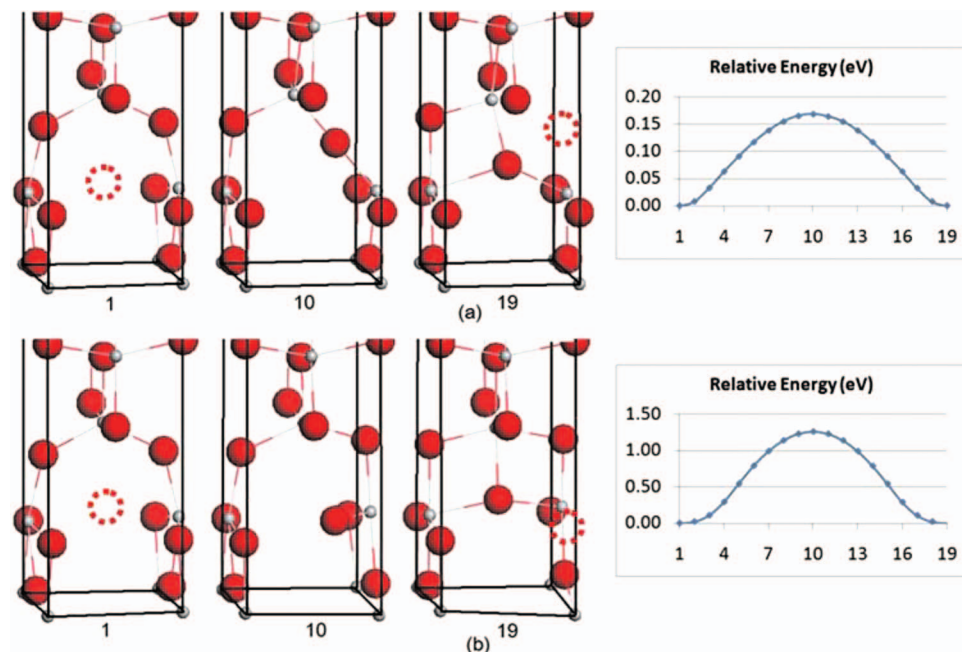


FIG. 3. The two basic diffusion pathways and the corresponding potential energy barriers for an oxygen vacancy in bulk anatase: (a) Diffusion from an apical to an equatorial position of a TiO$_6$ octahedron and (b) diffusion between two equatorial positions. Atomic structures are selected configurations along the minimum energy pathways shown on the right. Integers denote the different images in the NEB calculations of the pathways. The O atoms are red and Ti atoms are gray.

FIG. 4. Different possible Ti$_i$ defect sites at the A-TiO$_2$(101) surface. The O atoms are red, Ti atoms are gray, and the Ti interstitial is yellow.
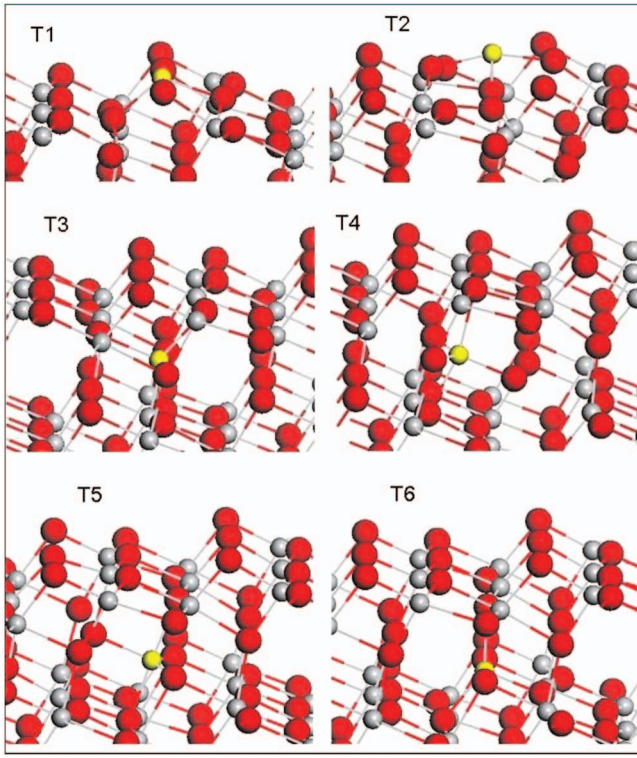
TABLE I. Formation energies $E_{form}$ and nearest-neighbor distances for Ti interstitials at different surface and subsurface sites of an anatase (101) slab (Fig. 4) and in bulk anatase calculated at the DFT-GGA level for oxygen rich conditions. The surface calculations were performed using a (101)-1×3 slab containing 108 atoms. The bulk calculations were performed using a $2\sqrt{2}\times2\sqrt{2}\times1$ bulk supercell containing 96 atoms. $K$-space was sampled at $\Gamma$ only.

| Defect site | $E_{form}$ (eV) | Distances to nearest oxygens (Å) |
|---|---|---|
| T1 | 8.87 | 1.889, 1.889, 1.930, 1.936 |
| T2 | 10.36 | 1.851, 1.887, 2.138, 2.140 |
| T3 | 8.69 | 1.960, 1.961, 2.007, 2.055, 2.056 |
| T4 | 8.42 | 1.806, 1.994, 1.998, 1.999, 2.052 |
| T5 | 7.76 | 1.891, 1.891, 1.910, 1.965, 1.990 |
| T6 | 7.62 | 1.847, 1.944, 1.948, 1.948, 1.952 |
| Bulk | 7.58 | 1.824, 1.921, 1.923, 1.954, 1.954 |

$\mu'_O=0$, which corresponds to the O-rich limit at which oxygen condensation occurs. We also assume that the entropic contributions to $G$ (def) and $G$ (no-def) cancel out in Eqs. (2) and (3); we thus approximate the free energy $G$ with the total ($T=0$ K) DFT energy $E_{tot}$. For $\mu_{TiO_2}$, we take the computed total energy of a TiO$_2$ unit in the bulk of anatase at $T=0$ K. As usual, our calculated GGA-PBE binding energy for the gas-phase O$_2$ molecule is overestimated, 6.64 eV, to be compared to the fully converged PBE value of 6.24 eV,[27] which is in turn ~1 eV larger than the experiment.

## III. DFT-GGA RESULTS FOR ANATASE TiO$_2$

### A. Bulk Ti$_i$ and $V_O$ defects

Anatase has a tetragonal lattice with four TiO$_2$ units per unit cell, see Fig. 1(a). The structure consists of chains of distorted TiO$_6$ octahedra. Each Ti atom is coordinated to the six neighboring oxygens via two (long) apical and four (short) equatorial bonds of lengths 1.973 and 1.930 Å (experimental values:[30] 1.979 and 1.932 Å), respectively. Each O atom is coordinated to three Ti atoms via one long bond and two short bonds lying in the same plane.

To study bulk defects, a nearly cubic $2\sqrt{2}\times2\sqrt{2}\times1$ (10.66×10.66×9.54 Å$^3$) bulk supercell containing 96 atoms was used; in the structural optimizations, all atomic positions were fully relaxed. The Brillouin zone was sampled using either a 2×2×2 $k$-point mesh or only $\Gamma$. Unlike the slab calculations, those for the bulk show a non-negligible dependence on $k$-sampling; this is due to both the relatively small size and the high symmetry of the bulk supercell.

The preferential binding site of an excess Ti atom in bulk anatase is found to be a highly coordinated pseudo-octahedral site. Upon relaxation, the top apical oxygen moves toward the Ti interstitial resulting in a very short Ti$_i$–O distance (1.824 Å), whereas the bottom apical O atom moves away from it [Fig. 1(b)]; in this way, both the defect atom and one lattice Ti close to it become fivefold coordinated. The computed defect formation energy is 8.43 eV (7.58 eV using only $\Gamma$).

The two basic diffusion pathways through which Ti$_i$ defects can move in the bulk are shown in Fig. 2. One pathway is along the [001] direction with an energy barrier of 0.78 eV and the other along [301] with a barrier of 0.45 eV. All other diffusion pathways result from a combination of these two basic pathways. Similar to the formation energies, also the Ti$_i$ diffusion barriers in anatase are not significantly different from those recently reported for interstitials in rutile.[33]

All O-vacancy sites in bulk anatase are equivalent. In the optimized structure, anisotropic atomic relaxations around the vacancy are present: one of the three nearest-neighbor Ti atoms moves away from the vacancy by 0.16 Å and the other two by 0.21 Å, while the two next-nearest-neighbor O atoms move toward the vacancy by 0.28 Å [Fig. 1(c)]. The computed formation energy of 4.41 eV (3.69 eV using only $\Gamma$) is similar to values obtained in previous theoretical studies of neutral O vacancies in bulk anatase[34,35] and rutile as well.[33] Thus it appears that the formation energy of O vacancies is much smaller than that of Ti interstitials. Accordingly,

TABLE II. Diffusion barriers ($E^A$) along the pathways connecting the various Ti interstitial binding sites shown in Fig. 4. The DFT-GGA calculations were performed using an anatase (101)-1×3 slab containing 108 atoms.

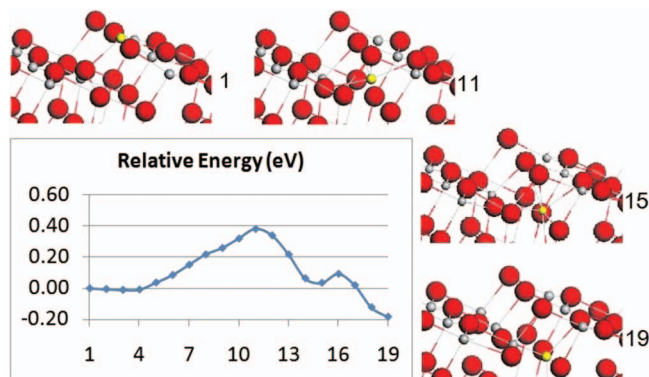| | $E^A$ (eV) for direct pathway | $E^A$ (eV) for inverse pathway | Diffusion direction |
|---|---|---|---|
| T1→T2 | 1.5 | 0 | |
| T1→T3 | 0.39 | 0.57 | [301] |
| T3→T4 | 0.14 | 0.41 | [001] |
| T4→T5 | 0.46 | 1.12 | [031] |
| T5→T6 | 0.04 | 0.19 | [001] |
| T3→T6 | 0.18 | 1.25 | [30$\bar{1}$] |

FIG. 5. Diffusion pathway from the surface T1 to the subsurface T3 site (see Fig. 4) for a Ti interstitial atom at the A-TiO$_2$(101) surface. Integers denote the different images in the NEB calculation of the pathway. The intermediate state represented by image 15 is a weakly metastable state. The O atoms are red, the Ti atoms are gray, and the Ti interstitial is yellow.

the $V_O$ defect concentration is expected to be higher than that of Ti interstitials under equilibrium conditions.

The two basic diffusion pathways of the O vacancy in bulk anatase are shown in Fig. 3. These correspond to jumps between corners of a TiO$_6$ octahedron. One pathway, in which the O vacancy jumps from an apical to an equatorial position, has a very low energy barrier $E^A = 0.17$ eV and should thus occur very frequently even at room temperature. The other pathway, in which the O vacancy jumps between equatorial positions, has a more substantial barrier $E^A = 1.26$ eV; however, a simple estimate indicates that also these processes are rather frequent at the annealing temperature of 900 K, $\nu \sim \nu_0 e^{-(E_a/kT)} \sim 10^5$ s$^{-1}$, using the typical value $\nu_0 \sim 10^{12}$ s$^{-1}$ for the attempt frequency.

## B. Surface and subsurface Ti interstitials

We identified several possible binding sites for an excess Ti atom on and near the A-TiO$_2$(101) surface (Fig. 4). The Ti$_i$–O distances and formation energies for these sites are reported in Table I. In the most stable surface binding site, denoted as T1, the Ti atom is in the middle between two adjacent O$_{2c}$ atoms along the [010] direction and is coordinated to four oxygens. Such a binding site has been found to be the most favorable one for other metal atoms on A-TiO$_2$(101) as well, e.g., for Pt. In all the subsurface sites the Ti interstitial is coordinated to five oxygen atoms, as in the bulk, and $E_{form}$ decreases as the defect moves away from the surface toward more bulklike sites with the values at T5 and T6 (the deepest sites that can be described with our slab model of 108 atoms) being very close to the formation energy of a Ti$_i$ defect in the bulk (computed using only $\Gamma$ as in the surface calculation). Note that the defect formation energy decreases by more than 1 eV from T3 to T6.

The diffusion pathways and barriers between the different Ti binding sites are reported in Table II. The pathway corresponding to the first diffusion step between surface and subsurface sites, namely, the path connecting T1 and T3, is reported in Fig. 5. This pathway is along the [301] direction like one of the two diffusion pathways in the bulk and has also a similar barrier of 0.39 eV (versus 0.45 eV in the bulk). Along this pathway we find a shallow local minimum state
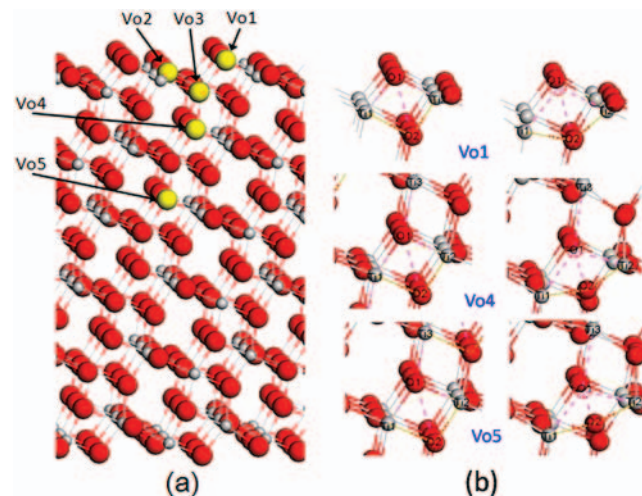


FIG. 6. (a) Slab model (216 atoms) and O-vacancy sites (highlighted in yellow) considered in this work. (b) Relaxed atomic structure before (left panels) and after (right panels) creation of an O vacancy at surface and subsurface sites of the A-TiO$_2$(101) surface. The positions of a few relevant atoms are indicated: O1 is the atom that is removed to create the defect; the position of this atom (before removal) is indicated by a dashed red circle in the panels on the right. Bond distances and angles for these six structures are given in Table IV.

represented by image 15 (we do not include this state among the local minima in Table I because the barrier to escape from it is very small less than 0.1 eV). From Table II, it also appears that after the first surface (T1)→subsurface (T3) diffusion step, subsequent steps, e.g., T3→T6, have barriers lower than 0.2 eV. By contrast, the reverse barrier from a subsurface site such as T5 or T6 to the surface is ∼1.25 eV, implying that Ti interstitials easily diffuse from the surface to inside the bulk, whereas it is unlikely that they move from the bulk toward the surface.

## C. Surface and subsurface O vacancies

As an introduction to the DFT+$U$ study of O vacancies in Sec. IV, we here summarize the DFT-GGA results that we recently reported in Ref. 23. The nonequivalent surface and subsurface oxygen sites at and near the A-TiO$_2$(101) surface are shown Fig. 6(a). In particular, these include three different surface oxygens, one twofold coordinated (O$_{2c}$), and two nonequivalent threefold coordinated sites. Table III reports the formation energies $E_{form}$ ($V_O$) computed using slab models of different sizes. Not surprisingly, $V_{O1}$ corresponding to an O$_{2c}$ vacancy is the energetically most favorable *surface*

TABLE III. Formation energies $E_{form}$ of $V_O$ defects at different surface and subsurface sites of an anatase (101) slab (Fig. 6) calculated at the DFT-GGA level for oxygen rich conditions. A $2 \times 2 \times 1$ $k$-point mesh was used in the case of the (101)-$2 \times 1$ slab containing 72 atoms, only $\Gamma$ in other cases.

| Defect site | $E_{form}$ (eV) $2 \times 1$-72 atoms | $E_{form}$ (eV) $3 \times 1$-108 atoms | $E_{form}$ (eV) $3 \times 1$-216 atoms |
|---|---|---|---|
| $V_{O1}$ | 4.39 | 4.25 | 4.15 |
| $V_{O2}$ | 5.43 | 5.40 | ⋯ |
| $V_{O3}$ | 4.95 | 4.73 | ⋯ |
| $V_{O4}$ | 4.18 | 4.03 | 3.69 |
| $V_{O5}$ | ⋯ | ⋯ | 3.65 |

TABLE IV. Relevant structural parameters before (A,B,C) and after (D,E,F) creation of a $V_O$ defect at the sites shown in Fig. 6(b). (A,D): $V_{O1}$; (B,E): $V_{O4}$; (C,F): $V_{O5}$.

| No. | O1–Ti1 (Å) | O1–Ti2 (Å) | O1–Ti3 (Å) | O1–O2 (Å) | Ti1–O2–Ti2 (deg) |
|---|---|---|---|---|---|
| A | 1.845 | 1.831 | ⋯ | 2.482 | 94.22 |
| B | 1.918 | 1.938 | 2.143 | 2.505 | 98.94 |
| C | 1.929 | 1.951 | 2.043 | 2.494 | 99.96 |
| D | 2.250 | 2.138 | ⋯ | 2.200 | 129.03 |
| E | 2.245 | 2.094 | 2.703 | 1.651 | 154.56 |
| F | 2.198 | 2.129 | 2.496 | 1.399 | 167.74 |

$V_O$ defect. Among subsurface sites, the site directly below $V_{O1}$ (not reported in Table III) is found to be unstable: if a vacancy is created at that site, the $O_{2c}$ atom just above it moves spontaneously to fill it, leaving a $V_{O1}$ vacancy. Most remarkably, the formation energy of the subsurface $V_{O4}$ defect is lower than that of $V_{O1}$. In particular, using a thick $(101)-1\times3$ slab containing 216 atoms (Fig. 6), the formation energies for the surface $V_{O1}$, first subsurface $V_{O4}$, and second subsurface $V_{O5}$ defects are 4.15, 3.69, and 3.65 eV, respectively. The values for the two subsurface defects are almost identical to the bulk $V_O$ formation energy (3.69 eV) that we obtained using only $\Gamma$ as for the surface calculations.

By comparing the results obtained with the thinner (108 atoms) and thicker (216 atoms) slabs in Table III, we can see that while $E_{form}$ for the surface $V_{O1}$ defect does not depend significantly on slab size, that for $V_{O4}$ is significantly smaller for the thicker slab, because this allows for a better local relaxation around the vacancy site. This result also provides the key for understanding why O vacancies prefer to stay in subsurface rather than at the surface. Indeed, analysis of the structural relaxations around the vacancy sites shows much larger atomic relaxations in the subsurface than at the surface, see Fig. 6(b) and Table IV; in particular, it appears that the change in the Ti1–O2–Ti2 angle upon relaxation is much larger for the subsurface sites than for the surface itself. The surface is very "rigid," as indicated also by the short bond lengths formed by $O_{2c}$ with the neighboring Ti atoms. These short bond lengths enhance the stability of the surface, but at the same time they also lead to a very high energy cost for creating a defect.

The O-vacancy pathways and diffusion barriers between the different surface and subsurface sites are reported in Table V. To obtain the optimal pathways, many initial guesses have been tested for each pair of initial and final O-vacancy states. Two pathways are listed for some of the pairs, e.g., for $V_{O1}\rightarrow V_{O2}$, because for a given initial site there are two possible nonequivalent final sites for the O vacancy. Some of the pathways involve collective movements that can be described as consisting of two diffusion events along two different directions. As an example, the $V_{O1}\rightarrow V_{O2}$ (2) pathway can be thought of as being composed of two of the simpler pathways: $V_{O1}\rightarrow V_{O3}$ (1) and $V_{O3}\rightarrow V_{O2}$. Vacancy diffusion on the surface appears to be largely inhibited: surface diffusion barriers are quite high, particularly the direct $V_{O1}\rightarrow V_{O1'}$ diffusion barrier of ~2.65 eV along [010]. This is very different in comparison

TABLE V. DFT-GGA diffusion barriers ($E^A$) along the pathways connecting the $V_O$ binding sites at or near the A-TiO$_2$(101) surface (Fig. 6). The calculations were performed using a (101)-2×1 slab containing 71 atoms.

| Pathway | $E^A$ (eV) for the direct pathway | $E^A$ (eV) for the inverse pathway | Diffusion direction |
|---|---|---|---|
| $V_{O1}\rightarrow V_{O1'}$ | 2.65 | 2.65 | [010] |
| $V_{O1}\rightarrow V_{O2}$ (1) | 1.52 | 0.47 | [021] |
| $V_{O1}\rightarrow V_{O2}$ (2) | 1.34 | 0.30 | [66$\bar{1}$]+[03$\bar{1}$] |
| $V_{O1}\rightarrow V_{O3}$ (1) | 1.34 | 0.78 | [66$\bar{1}$] |
| $V_{O1}\rightarrow V_{O3}$ (2) | 1.52 | 0.96 | [0$\bar{2}$1]+[031] |
| $V_{O2}\rightarrow V_{O3}$ | 0.30 | 0.78 | [031] |
| $V_{O1}\rightarrow V_{O4}$ | 0.74 | 0.95 | [301]+[30$\bar{1}$] |
| $V_{O2}\rightarrow V_{O4}$ (1) | 1.55 | 2.80 | [201] |
| $V_{O2}\rightarrow V_{O4}$ (2) | 0.30 | 1.56 | [031]+[66$\bar{1}$] |
| $V_{O3}\rightarrow V_{O4}$ | 0.78 | 1.56 | [661] |

with R-TiO$_2$(110), where STM measurements and DFT calculations found that bridge-bonded oxygen vacancies diffuse on the surface with an activation energy of ~1.1 eV.[36]

In contrast to diffusion on the surface, the diffusion of the O vacancy is quite easy from the surface $V_{O1}$ to the subsurface $V_{O4}$ site; the barrier is only 0.74 eV. This indicates that this pathway can be easily accessed under annealing conditions, thus allowing for rapid equilibration of the defect density between surface and subsurface sites. Selected atomic configurations along the pathway are shown in Fig. 7. We can see a two-atom diffusion mechanism, in which the sub-bridging oxygen (i.e., the O atom directly below $O_{2c}$) moves up to fill the $V_{O1}$ vacancy while the site that it leaves vacant is filled by the O atom initially in the $V_{O4}$ site. Note that Table V reports a barrier of 0.95 eV for the reverse $V_{O4}\rightarrow V_{O1}$ process. Taking into account that the 72 slab
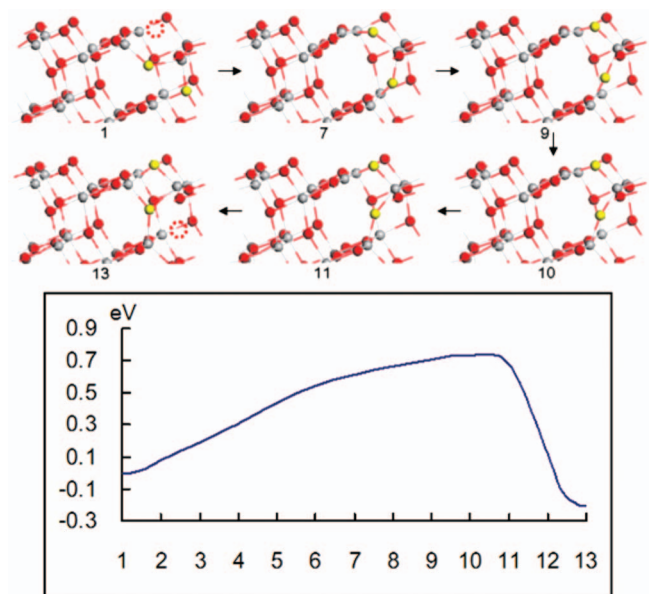


FIG. 7. Potential energy profile along the $V_{O1}\rightarrow V_{O4}$ diffusion pathway. In the upper part of the figure selected atomic configurations (NEB "images") along the pathway are shown. The initial and final positions of the vacancy are indicated by a dashed red circle; the two oxygens which undergo the large displacements in the diffusion process are highlighted in yellow.

TABLE VI. Formation energies ($E_{form}$), total magnetization ($S \equiv |\int [n_\uparrow(\mathbf{r}) - n_\downarrow(\mathbf{r})]d\mathbf{r}|$, where $n_\uparrow(\mathbf{r})$ and $n_\downarrow(\mathbf{r})$ are the densities of spin-up and spin-down electrons, and the integral is extended over the simulation cell), and energy levels relative to the bottom of the conduction band ($\varepsilon 1, \varepsilon 2$) for surface ($V_{O1}$) and subsurface ($V_{O4}$) oxygen vacancies at the anatase (101) surface calculated at the DFT+$U$ level using different values of $U$. $E_G$ is the computed energy gap (experimental value of 3.2 eV). All energies are in eV. Noninteger values of $S$ indicate spin contamination.

| $U$ | $E_G$ | $V_{O1}$ | | | $V_{O4}$ | | |
|---|---|---|---|---|---|---|---|
| | | $E_{form}$ | $S$ | $-\varepsilon 1, -\varepsilon 2$ | $E_{form}$ | $S$ | $-\varepsilon 1, -\varepsilon 2$ |
| 4.5 | 3.1 | 3.39 | 2.1 | 2.03, 1.82 | 3.72 | 2.1 | 1.71, 1.26 |
| 3.5 | 2.9(5) | 3.87 | 2.0 | 1.47, 1.24 | 4.14 | 2.1 | 1.17, 0.99 |
| 3.0 | 2.9 | 4.12 | 2.0 | 1.20, 0.95 | 4.11 | 0.0 | 0.60, 0.58 |
| 2.5 | 2.8(5) | 4.34 | 2.0 | 0.95, 0.68 | 4.20 | 0.0 | 0.41, 0.32 |

model used for the barrier calculations underestimates the relative stability of the $V_{O1}$ and $V_{O4}$ sites by $\sim 0.3$ eV (compare the results for 72 and 216 atom slabs in Table III), a more realistic estimate for the $V_{O4} \rightarrow V_{O1}$ diffusion barrier is $\sim 1.2$ eV. This suggests that the reverse subsurface $\rightarrow$ surface diffusion is quite unlikely, i.e., defects tend to remain confined in the subsurface region. To further verify the accuracy of the transition state for this pathway we relaxed nearby structures at the two sides of the saddle point; these structures relaxed indeed either toward the initial or the final state of the pathway, confirming the reliability of the transition state.

## IV. DFT+$U$ CALCULATIONS OF THE RELATIVE STABILITY OF SURFACE ($V_{O1}$) AND SUBSURFACE ($V_{O4}$) DEFECTS AT THE A-TiO$_2$(101) SURFACE

The DFT-GGA calculations in Sec. III predict that the subsurface $V_{O4}$ and $V_{O5}$ defects are more stable than $V_{O1}$, the surface O$_{2c}$ vacancy, as a result of the larger and more favorable local lattice relaxation around the former defects. As mentioned in Sec. I, however, the electronic structure of $V_O$ defects is not well described by DFT-GGA. According to this approach, indeed, the electronic states associated with these defects lie at the bottom of the TiO$_2$ conduction band. Instead, experiments show that their energies are in the gap; moreover, there is evidence that these states are quite localized and have a polaronic character, see, e.g., Refs. 12, 15, 17, and 18 and references therein. The polaronic distortion can interfere with the atomic relaxation around the defect and possibly modify the relative stability of surface and subsurface defects predicted at the DFT-GGA level.

To investigate the effect of the (partial) localization of the defect electronic states on the relative energetics of surface $V_{O1}$ and subsurface $V_{O4}$ defects, we have carried out spin-polarized DFT+$U$ calculations on A-TiO$_2$(101) slabs of four TiO$_2$ layers (96 atoms) using different values of $U$, namely, $U=4.5$, 3.5, 3.0, and 2.5 eV, that encompass the range of values typically found for TiO$_2$.[15,21] These values are also consistent with a recent theoretical estimate by Mattioli *et al.*,[22] who obtained $U=3.3$ (3.4) eV for anatase (rutile) using a computational setup very similar to that adopted in the present work. For each $U$, two different starting atomic configurations were fully optimized, the defected
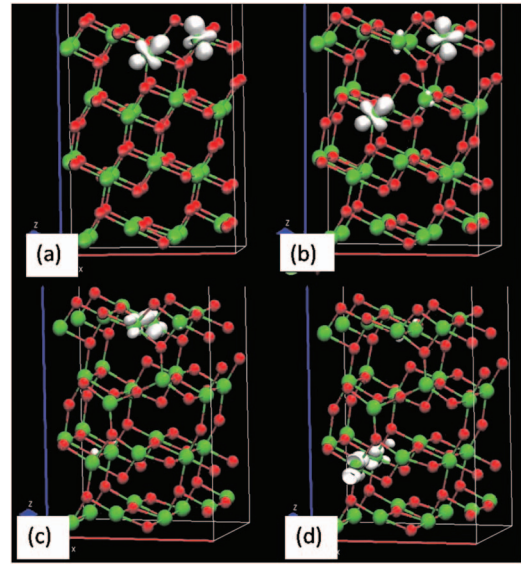


FIG. 8. Spin density isosurfaces ($10^{-2}$ a.u.$^{-3}$) from DFT+$U$ calculations of $V_{O1}$ and $V_{O4}$ defects in A-TiO$_2$(101). [(a) and (b)] Triplet states of $V_{O1}$ and $V_{O4}$, respectively, computed using $U=3.5$ eV. [(c) and (d)] $V_{O4}$ components of the spin-singlet state obtained with $U=3$ eV. The O atoms are red and the Ti atoms are green.

unrelaxed slab and the defected slab relaxed at the DFT-GGA level; in both cases, various choices of the initial magnetization were considered. Our results are summarized in Table VI, where the formation energies $E_{form}$ and total magnetizations $S$ of the $V_{O1}$ and $V_{O4}$ containing slabs are reported for different values of $U$ (here $S \equiv |\int [n_\uparrow(\mathbf{r}) - n_\downarrow(\mathbf{r})]d\mathbf{r}|$, where $n_\uparrow(\mathbf{r})$ and $n_\downarrow(\mathbf{r})$ are the densities of spin-up and spin-down electrons, and the integral is extended over the simulation cell); also shown are the defect levels ($\varepsilon 1, \varepsilon 2$) in the band gap relative to the conduction band edge. The results in this table have been confirmed by selected calculations for a larger slab of 144 atoms.

Inspection of Table VI shows differences in the defect properties for large and small values of $U$. For larger values, namely, $U=4.5$ and 3.5 eV, the excess electrons of both $V_{O1}$ and $V_{O4}$ defects form a triplet state with each electron localized at a single Ti site as evident from the spin density plots in Figs. 8(a) and 8(b). For $V_{O1}$, the two excess electrons localize at the two undercoordinated surface Ti atoms adjacent to the vacant O$_{2c}$ site (note that these Ti atoms are relaxed outward from the vacancy, so that the distance between them is larger than on the stoichiometric surface), whereas for $V_{O4}$ only one of the two electrons localizes at a Ti adjacent to the vacancy; the other moves to an undercoordinated surface Ti atom, causing some distortion of its bonds to the neighboring oxygens. The energetic cost of this distortion has the effect of destabilizing $V_{O4}$ by $\sim 0.3$ eV relative to $V_{O1}$. For smaller values of $U$, around $U=3.0$ eV a crossover of the stabilities of $V_{O1}$ and $V_{O4}$ takes place, and $V_{O4}$ becomes slightly more stable than $V_{O1}$ at $U=2.5$ eV. Moreover, while the electronic states associated with $V_{O1}$ maintain the character of a triplet with the two electrons localized as in Fig. 8(a), at $U=3$ eV the characters of the $V_{O4}$ states change: they become somewhat more delocalized,

TABLE VII. Formation energies $E_{form}$ of $V_O$ defects at different surface and subsurface sites of a R-TiO$_2$(110) slab (Fig. 9) calculated at the DFT-GGA level for oxygen rich conditions. Calculations were performed using a $c(4 \times 2)$ surface supercell. $K$-space was sampled using only $\Gamma$.

| Defect site | $E_{form}$ (eV) | |
|---|---|---|
| | 96 atom slab | 144 atom slab |
| $V_{O1}$ | 4.01 | 3.68 |
| $V_{O2}$ | 4.56 | 4.50 |
| $V_{O3}$ | 4.23 | 3.99 |
| $V_{O4}$ | 5.22 | 5.23 |
| $V_{O5}$ | 4.83 | 4.73 |
| $V_{O6}$ | 5.29 | 5.28 |
| $V_{O7}$ | | 4.46 |
| $V_{O8}$ | | 4.67 |
| $V_{O9}$ | | 4.38 |



FIG. 9. Slab model with six TiO$_2$ layers and O-vacancy sites (highlighted in yellow) of the R-TiO$_2$(110) surface considered in this work. For simplicity, the unrelaxed slab is shown. Oxygens are red and Ti atoms are gray.

one at the surface and the other in the layer below the O vacancy [Figs. 8(c) and 8(d)], and form an open-shell singlet.

Turning now to an analysis of defect energy levels, from Table VI we can see that for all values of $U$ the energy levels $\varepsilon1$ and $\varepsilon2$ of $V_{O4}$ are about 0.3–0.5 eV closer to the conduction band than the corresponding levels of $V_{O1}$, suggesting that the $V_{O4}$ defect states have a greater tendency to become delocalized. In the case $U=4.5$ eV, however, the energy levels of both $V_{O1}$ and $V_{O4}$ are considerably too low with respect to the experimental value of $\sim0.9$ eV,[11,17] indicating that this value of $U$ is too large for A-TiO$_2$(101). The situation is somewhat more complicated in the case of $U=3.5$ eV: the $V_{O1}$ energy levels are still too low, whereas those of $V_{O4}$ could be considered compatible with the experiment. For $U \leq 3$ eV, however, i.e., when the $V_{O4}$ states become more delocalized, the corresponding energy levels become quite shallow ($\leq0.6$ eV) and not consistent with the experimental estimate of $\sim0.9$ eV. Vice versa, for $U=3$ eV, it is $V_{O1}$ which shows levels in agreement with experiment.

In summary, our DFT+$U$ calculations on surface $V_{O1}$ and subsurface $V_{O4}$ defects at A-TiO$_2$(101) show a complex behavior with a crossover in the relative stabilities of $V_{O1}$ and $V_{O4}$ as a function of $U$. Quite interestingly, for the range of $U$ values which provide the best description of the energy levels as compared to experiments, namely, $3 \leq U \leq 3.5$ eV, $V_{O1}$ and $V_{O4}$ appear to have a comparable stability.

## V. SURFACE AND SUBSURFACE O VACANCIES IN R-TiO$_2$(110)

For comparison with our results for the reduced A-TiO$_2$(101) surface, we have studied the relative stabilities of surface and subsurface O vacancies also at R-TiO$_2$(110), a surface for which a large number of experimental and theoretical results are already available. To this end, we performed DFT-GGA and spin-polarized DFT+$U$ calculations on R-TiO$_2$(110) slabs of four and six TiO$_2$ layers containing 96 and 144 atoms, respectively [see Fig. 9]. We used a $c(4 \times 2)$ ($8.84 \times 8.84$ Å$^2$ with an angle of 84.2°) surface supercell in which the periodic images of the vacancies are
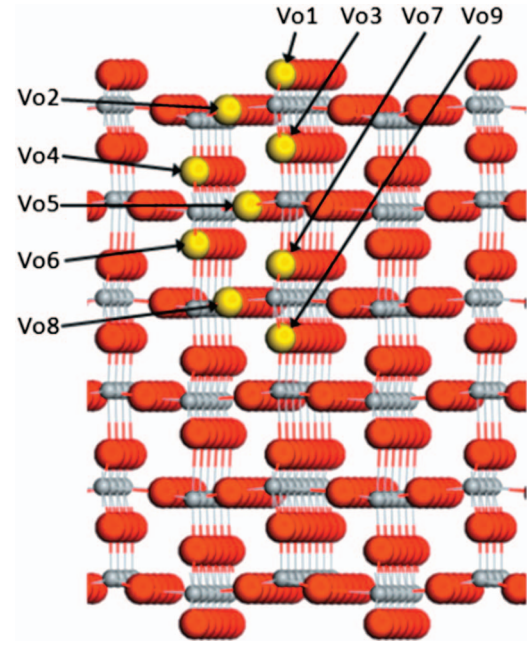
staggered, so that their nearest-neighbor distance is larger than in other surface supercell of the same area.[16] The rest of the computational setup was identical to that used for the A-TiO$_2$(101) surface.

At the DFT-GGA level, the defect formation energies for the first O–Ti–O trilayer of R-TiO$_2$(110) are the lowest ones, whereas those for the second trilayer are quite high (see Table VII) in agreement with previous calculations.[24,26] These results suggest that most O vacancies should occur at the $V_{O1}$ bridging and $V_{O3}$ sub-bridging sites on R-TiO$_2$(110). Unlike O vacancies on anatase (101), the surface $V_{O1}$ defect gives rise to a triplet state on rutile (110).

The spin-polarized DFT+$U$ calculations were carried out only for the $V_{O1}$ and subsurface $V_{O4}$ vacancies (see Fig. 9) using slabs of four TiO$_2$ layers (96 atoms) and three different values of $U$, namely, $U=3$, 3.5, and 4.5 eV. For each $U$, two different starting atomic configurations were optimized, the defected unrelaxed slab and the defected slab relaxed at the DFT-GGA level. The results are summarized in Table VIII and Fig. 10. It appears that at variance with the case of A-TiO$_2$(101), for R-TiO$_2$(110) there is no crossover

TABLE VIII. Formation energies ($E_{form}$), total magnetization ($S$), and energy levels relative to the bottom of the conduction band ($\varepsilon1, \varepsilon2$) for surface ($V_{O1}$) and subsurface ($V_{O4}$) oxygen vacancies at the R-TiO$_2$(110) surface calculated at the DFT+$U$ level using different values of $U$. $E_G$ is the computed energy gap (experimental value of $\sim3$ eV). All energies are in eV. Noninteger values of $S$ indicate the occurrence of spin contamination.

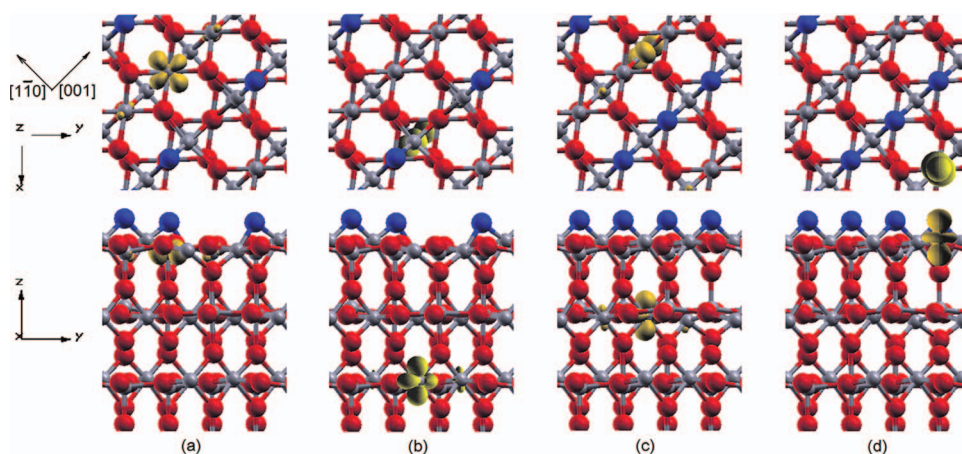| | | $V_{O1}$ | | | $V_{O4}$ | | |
|---|---|---|---|---|---|---|---|
| $U$ | $E_G$ | $E_{form}$ | $S$ | $-\varepsilon1, -\varepsilon2$ | $E_{form}$ | $S$ | $-\varepsilon1, -\varepsilon2$ |
| 4.5 | 2.4 | 2.88 | 0 | 1.68, 1.43 | 3.39 | 0.3 | 2.36, 1.99 |
| 3.5 | 2.3 | 3.26 | 0 | 1.22, 0.83 | 3.84 | 0.1 | 2.31, 1.35 |
| 3.0 | 2.2 | 3.34 | 0.1 | 0.45, 0.41 | 4.11 | 0.3 | 2.13, 1.04 |

FIG. 10. Top and side views of the spin density isosurfaces ($10^{-2}$ a.u.$^{-3}$) of $V_{O1}$ and $V_{O4}$ defect states in R-TiO$_2$(110) obtained from DFT+$U$ calculations with $U$=3.5 eV. [(a) and (b)] $V_{O1}$. [(c) and (d)] $V_{O4}$. For better clarity, the surface bridging oxygens are shown in blue, while all other oxygens are in red; the Ti atoms are gray.

of the stabilities of $V_{O1}$ and $V_{O4}$ when $U$ is varied: the formation energy of $V_{O1}$ is always about 0.5 eV lower than that of $V_{O4}$. Also at variance with A-TiO$_2$(101), for all values of $U$ the energy levels $\varepsilon 1$ and $\varepsilon 2$ of $V_{O1}$ are closer to the conduction band than the corresponding levels of $V_{O4}$. In all investigated cases, both $V_{O1}$ and $V_{O4}$ prefer to form an open-shell singlet state even though the triplet state is often very close in energy. In the case of the surface $V_{O1}$ defect, both electronic states are delocalized and close to the conduction band edge for $U$=3 eV; for $U$=3.5 and 4.5 eV, instead, they are both localized, one at a fivefold Ti in the first layer and the other at a sixfold Ti in the third layer (Fig. 10). The $V_{O1}$ defect energy levels for $U$=3.5 eV lie at ~0.8 and 1.2 eV below the conduction band edge in agreement with the experimental value of ~0.9 eV. For comparison, we note that the localization of the $V_{O1}$ defect states at two nonequivalent surface Ti sites was found in the hybrid functional study of Ref. 12. In the case of the subsurface $V_{O4}$ defect, the two electrons are both localized, independent of the value of $U$; one state is at a surface fivefold Ti, while the other is in the second layer on a Ti atom next nearest neighbor to the O vacancy (see Fig. 10). Curiously, the energy level of the state localized at a surface Ti is always close to the top of valence band, and this Ti atom shows an outward relaxation of ~0.3 Å. Altogether, the DFT+$U$ results for reduced R-TiO$_2$(110) confirm the presence of important differences between this surface and reduced A-TiO$_2$(101) as found in the DFT-GGA calculations.

## VI. CONCLUSIONS

The results in Secs. III–V provide evidence of a key role of subsurface defects, notably O vacancies and Ti interstitials, at the reduced A-TiO$_2$(101) surface. At the DFT-GGA level, the difference in stability between surface and subsurface sites is $\Delta E \sim 1.2$ eV for Ti interstitials and $\Delta E \sim 0.5$ eV for O vacancies. Moreover, the surface →subsurface diffusion barriers for both Ti$_i$ and $V_O$ are less than or near 1 eV. Thus, once formed, these defects should easily diffuse toward the bulk. Calculations of surface and subsurface O-vacancy formation energies for the rutile (110) surface yield results very different from those for anatase (101): on R-TiO$_2$(110), O$_{2c}$ vacancies are clearly more likely to occur than subsurface vacancies. The results of our DFT

+$U$ calculations on the relative stabilities of surface $V_{O1}$ and subsurface $V_{O4}$ defects show a more complex behavior with a crossover of the relative stabilities of $V_{O1}$ and $V_{O4}$ as a function of $U$ in A-TiO$_2$(101). Still, also at the DFT+$U$ level our results confirm the presence of important differences between the reduced R-TiO$_2$(110) and A-TiO$_2$(101) surfaces with a clearly more prominent role of subsurface defects for the latter.

These differences between anatase and rutile have some important consequences. First, they can explain the low concentration of O vacancies observed by STM[8,9] and TPD (Ref. 10) on the anatase (101) surface. They are also consistent with the UPS data showing numerous gap states following bombardment and annealing of the anatase (101) surface.[11] In fact, the observed defect states can be assigned to vacancies in the subsurface region, which is accessed by UPS measurements and where the $V_O$ defects prefer to reside according to our calculations. Differences between A-TiO$_2$(101) and R-TiO$_2$(110) can be also explained along the lines proposed in Ref. 23. Second, we notice that subsurface defects are less reactive than surface oxygen vacancies. The latter is quickly quenched by adsorption of molecules from the environment, whereas subsurface vacancies can have a much longer lifetime. In TiO$_2$-based photocatalysis[1] defects act as trap sites for photoexcited charge carriers. Thus O vacancies located just beneath the top surface layer could steer photoexcited charge carriers to near-surface regions. This could contribute to the superior photocatalytic properties of anatase with respect to rutile.

[1] A. L. Linsebigler, G. Lu, and J. T. Yates, Jr., Chem. Rev. (Washington, D.C.) **95**, 735 (1995).
[2] M. R. Hoffmann, S. T. Martin, W. Choi, and D. W. Bahnemann, Chem. Rev. (Washington, D.C.) **95**, 69 (1995).
[3] T. L. Thompson and J. T. Yates, Chem. Rev. (Washington, D.C.) **106**, 4428 (2006).
[4] B. O'Regan and M. Grätzel, Nature (London) **353**, 737 (1991).
[5] M. Grätzel, Nature (London) **414**, 338 (2001).

[6] M. Lazzeri, A. Vittadini, and A. Selloni, Phys. Rev. B **63**, 155409 (2001).

[7] U. Diebold, N. Ruzycki, G. S. Herman, and A. Selloni, Catal. Today **85**, 93 (2003).

[8] W. Hebenstreit, N. Ruzycki, G. S. Herman, Y. Gao, and U. Diebold, Phys. Rev. B **62**, R16334 (2000).

[9] Y. He, O. Dulub, H. Cheng, A. Selloni, and U. Diebold, Phys. Rev. Lett. **102**, 106105 (2009).

[10] G. S. Herman, Z. Dohnalek, N. Ruzycki, and U. Diebold, J. Phys. Chem. B **107**, 2788 (2003).

[11] A. G. Thomas, W. R. Flavell, A. K. Mallick, A. R. Kumarasinghe, D. Tsoutsou, N. Khan, C. Chatwin, S. Rayner, G. C. Smith, R. L. Stockbauer, S. Warren, T. K. Johal, S. Patel, D. Holland, A. Taleb, and F. Wiame, Phys. Rev. B **75**, 035105 (2007).

[12] C. Di Valentin, G. Pacchioni, and A. Selloni, Phys. Rev. Lett. **97**, 166803 (2006).

[13] V. M. Ganduglia-Pirovano, A. Hofmann, and J. Sauer, Surf. Sci. Rep. **62**, 219 (2007).

[14] C. J. Calzado, N. C. Hernandez, and J. F. Sanz, Phys. Rev. B **77**, 045118 (2008).

[15] E. Finazzi, C. Di Valentin, G. Pacchioni, and A. Selloni, J. Chem. Phys. **129**, 154113 (2008).

[16] M. D. Rasmussen, L. M. Molina, and B. Hammer, J. Chem. Phys. **120**, 988 (2004).

[17] U. Diebold, Surf. Sci. Rep. **48**, 53 (2003).

[18] P. Kruger, S. Bourgeois, B. Domenichini, H. Magnan, D. Chandesris, P. L. Fevre, A. M. Flank, J. Jupille, L. Floreano, A. Cossaro, A. Verdini, and A. Morgante, Phys. Rev. Lett. **100**, 055501 (2008).

[19] A. J. Cohen, P. Mori-Sanchez, and W. Yang, Science **321**, 792 (2008).

[20] V. I. Anisimov, J. Zaanen, and O. K. Andersen, Phys. Rev. B **44**, 943 (1991).

[21] B. J. Morgan and G. W. Watson, Surf. Sci. **601**, 5034 (2007).

[22] G. Mattioli, F. Filippone, P. Alippi, and A. A. Bonapasta, Phys. Rev. B **78**, 241201 (2008).

[23] H. Cheng and A. Selloni, Phys. Rev. B **79**, 092101 (2009).

[24] J. Oviedo, M. A. San Miguel, and J. F. Sanz, J. Chem. Phys. **121**, 7427 (2004).

[25] K. Hameeuw, G. Cantele, D. Ninno, F. Trani, and G. Iadonisi, Phys. Status Solidi A **203**, 2219 (2006).

[26] T. Pabisiak and A. Kiejna, Solid State Commun. **144**, 324 (2007).

[27] J. P. Perdew, K. Burke, and M. Ernzerhof, Phys. Rev. Lett. **77**, 3865 (1996).

[28] S. Baroni, P. Giannozzi, S. De Gironcoli, and A. Dal Corso, QUANTUM ESPRESSO, http://www.democritos.it.

[29] D. Vanderbilt, Phys. Rev. B **41**, 7892 (1990).

[30] J. K. Burdett, T. Hughbanks, G. J. Miller, J. W. Richardson, and J. V. Smith, J. Am. Chem. Soc. **109**, 3639 (1987).

[31] G. Henkelman, B. P. Uberuaga, and H. Jonsson, J. Chem. Phys. **113**, 9901 (2000).

[32] K. Reuter and M. Scheffler, Phys. Rev. B **68**, 045407 (2003).

[33] H. Iddir, S. Ogut, P. Zapol, and N. D. Browning, Phys. Rev. B **75**, 073203 (2007).

[34] C. Di Valentin, G. Pacchioni, A. Selloni, S. Livraghi, and E. Giamello, J. Phys. Chem. B **109**, 11414 (2005).

[35] S. Na-Phattalung, M. F. Smith, K. Kwiseon, D. Mao-Hua, W. Su-Huai, S. B. Zhang, and L. Sukit, Phys. Rev. B **73**, 125205 (2006).

[36] Z. Zhang, Q. Ge, S.-C. Li, B. D. Kay, J. M. White, and Z. Dohnalek, Phys. Rev. Lett. **99**, 126105 (2007).